Photochemical etiology of promising ancestors of the RNA nucleobases

Matthew M. Brister,[a] Marvin Pollum,[a] and Carlos E. Crespo-Hernández[a],*

[a] Department of Chemistry and Center for Chemical Dynamics, Case Western Reserve University, Cleveland, Ohio 44106, United States

* Email: carlos.crespo@case.edu

Revised Electronic Supporting Information

1. Materials and Spectroscopic Methods

Barbituric acid (BA) (99% purity) and 2,4,6-triaminopyrimidine (TAP) (97% purity) were used as received from Sigma-Aldrich. Monosodium and disodium phosphate salts (99.0% purity, Sigma-Aldrich) were used to make a phosphate buffered saline (PBS) solution at a total salt concentration of 50 mM. The pH was adjusted with 0.1 M sodium hydroxide and phosphoric acid (Fisher Chemical, certified ACS grade ≥ 85 % w/w) to the desired pH (± 0.1 pH units). The experimental setup and data analysis have been discussed in detail elsewhere.[1–3] Briefly, the fundamental laser beam of 800 nm at a 1 kHz repetition rate (4.1 W, 100 fs pulse, Libra-HE, Coherent Inc.) was split in two by a 90/10 beam splitter. Ninety percent of the fundamental was directed into an optical parametric amplifier (TOPAS, Quantronix/Light Conversion) and converted into 268 nm laser pulse by second-harmonic sum frequency generation. The 268 nm laser pulse was used as the excitation wavelength for the molecular systems. A small fraction of the other ten percent of the fundamental was used to generate a white light continuum in the spectral window of 320 to 700 nm by orthogonally passing the 800 nm beam through a 2 mm thick CaF_2 crystal. The instrument response function was estimated from the coherence signal of pure methanol, which was determined to be 200 ± 50 fs.[4] Time zero was set at the maximum

absorption signal of the initially-observed absorption band in the visible region for BA (~500 nm) and TAP (~600 nm). Homogeneity of the solutions was achieved by using a Teflon-coated magnetic stir bar in a 2 mm fused silica cuvette. Freshly prepared solution was used each time that more than 5% photodegradation of the solute occurred, as judged by steady-state absorption spectroscopy (Cary 100 Bio Instrument, Agilent Technologies). The potential formation of hydrated electrons from two-photon absorption by the water solvent was avoided by using optical densities for the solute in the range of 2 to 2.5 at the excitation wavelength, and simultaneously attenuating the photon flux of the pump pulse, as judged by a back-to-back probing of adenosine monophosphate at the same optical density at the excitation wavelength, as reported elsewhere.[5]

2.   *Computational Methods*

All calculations were performed using the Gaussian 09 suite of programs.[6] Solvent effects were modeled using the self-consistent reaction field (SCRF) model with the integral equation formalism of the polarized continuum model (IEF-PCM).[7,8] Unless stated otherwise, the ground-state structures were optimized using the B3LYP functional with a 6-311++G(d,p) standard basis set and no symmetry constraints. Vibrational frequency calculations were preformed to ensure that all optimized structures show only positive frequencies. All optimized structures are planar with the exception of tautomers 2 and 9, as shown with a side view in Figure S1. This figure shows the optimized structures obtained in water using the IEF-PCM reaction field. Table S1 depicts the ordered energies of each tautomer of BA relative to the most stable tautomer (i.e., the tri-keto) within the water solvation model used. Also represented are the energies of each tautomer of BA relative to the most stable tautomer (tri-keto) using acetonitrile solvation model.

Ground-state optimizations were also performed for the five lowest-energy tautomers of BA obtained within the water solvation model, as reported in Table S1, but complexed with three explicit water molecules (Figure S2). The M06 functional, which is optimized for hydrogen bonding interactions,[9] and the 6-31+G(d,p) basis set were used for these micro-hydration calculations without any symmetry constraints. Most of the optimized structures exhibit a slight deformation from planarity (Figure S2). Table S2 shows the calculated energies and the corresponding dipole moments at the M06/6-31+G(d,p) level of theory and single-point calculations at the B3LYP/IEF-PCM/6-311++G(d,p)||M06/6-31+G(d,p) level of theory.

The time-dependent implementation of density functional theory (TD-DFT) with the PBE0 functional and a 6-311++G(d,p) basis set was used to model the vertical excitation energies.[10,11] The characters of the excited states were estimated through (1) visual inspection of the Kohn-Sham orbitals; (2) the effect of solvent on the excited-state energies; and (3) the magnitude of the oscillator strengths. The vertical excitation energies for the tri-keto tautomer of BA and TAP are given in Tables S3 and S9 in vacuum, acetonitrile, and water. The bulk solvent effects were modeled within the IEF-PCM reaction field model.

For the optimized micro-hydrated structures (Figure S2), vertical excitation energies were calculated at the TD-PBE0/IFE-PCM/6-311++G(d,p) level using the water solvation model. The characters of the vertical excited states were estimated through visual inspection of the Kohn-Sham orbitals and the magnitude of the oscillator strengths (Tables S4 to S8).

The vertical excitation energies shown in Figures S4, S5, and S8 were red shifted to match the lowest-energy absorption band of BA or TAP, as described in each figure, in order to provide a clearer comparison with the experimentally-obtained ground-state absorption spectra.

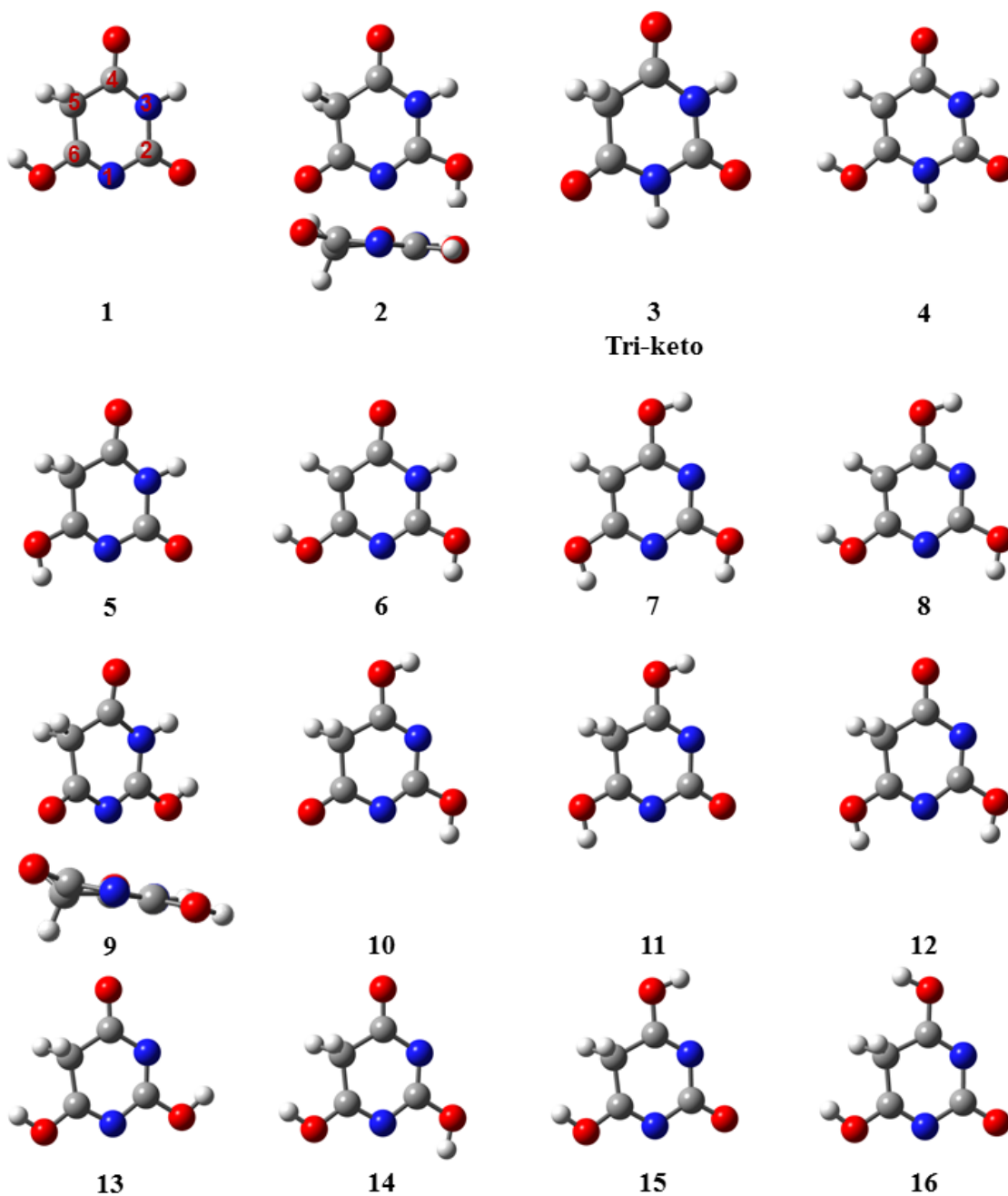## 3. *Barbituric Acid*

3.1 *Computational Results*

Figure S1. Optimized ground state geometries of the 16 tautomers of barbituric acid as determined at the B3LYP/IEF-PCM/6-311++G(d,p) level of theory in water.

Revised Table S1.[a] Energy of the optimized ground state of the 16 tautomers of barbituric acid relative to the lowest energy tautomer, tri-keto, determined at the B3LYP/IEF-PCM/6-311++G(d,p) level of theory in water and energy of the optimized ground state of the 16 tautomers of barbituric acid relative to the lowest energy tautomer, tri-keto, determined at the B3LYP/IEF-PCM/6-311++G(d,p) level of theory in acetonitrile.

	Water		Acetonitrile	
Tautomer	**Energy (kJ/mol)**	**Dipole Moment (Debye)**	**Energy (kJ/mol)**	**Dipole Moment (Debye)**
1	73.05	7.27	73.79	7.21
2	76.54	5.27	76.75	5.22
3	**0.00**	**0.05**	**0.00**	**0.08**
4	33.66	6.53	33.85	6.48
5	59.94	4.76	60.09	4.72
6	78.93	3.50	79.03	3.48
7	88.50	1.94	88.11	1.93
8	95.74	7.97	96.67	7.90
9	95.77	3.15	95.68	3.12
10	127.54	5.62	127.74	5.57
11	127.86	7.82	128.25	7.74
12	130.13	9.48	130.65	9.41
13	138.42	5.15	139.12	5.10
14	140.31	8.56	141.16	8.49
15	141.06	11.24	142.15	11.14
16	154.95	14.36	156.81	14.22

[a] The energetic ordering reported in the originally-submitted Table S1 for the 16 tautomers of BA using the water solvation model was incorrect (a tabulation error), where the enol(C6) was shown as the lowest-energy tautomer instead of the tri-keto tautomer. Similarly, the energetic ordering for the 16 tautomers of BA using the acetonitrile solvation model was (a tabulation error), but the lowest-energy tautomer remains the tri-keto tautomer, as in the original table.
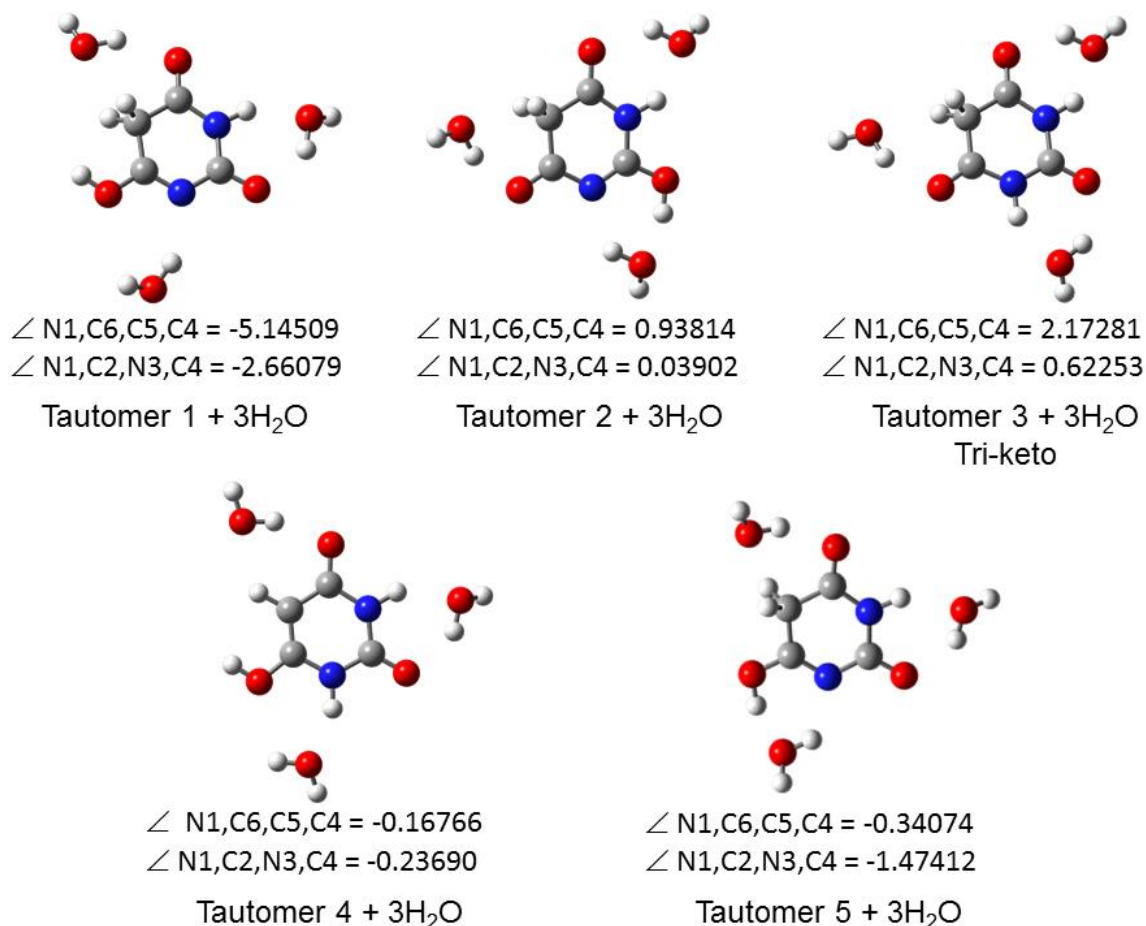
∠ N1,C6,C5,C4 = -5.14509
∠ N1,C2,N3,C4 = -2.66079

Tautomer 1 + 3H$_2$O

∠ N1,C6,C5,C4 = 0.93814
∠ N1,C2,N3,C4 = 0.03902

Tautomer 2 + 3H$_2$O

∠ N1,C6,C5,C4 = 2.17281
∠ N1,C2,N3,C4 = 0.62253

Tautomer 3 + 3H$_2$O
Tri-keto

∠ N1,C6,C5,C4 = -0.16766
∠ N1,C2,N3,C4 = -0.23690

Tautomer 4 + 3H$_2$O

∠ N1,C6,C5,C4 = -0.34074
∠ N1,C2,N3,C4 = -1.47412

Tautomer 5 + 3H$_2$O

Figure S2. Optimized ground-state structures for the five lowest-energy tautomers of barbituric acid in water (Table S1), complexed with 3H$_2$O molecules, obtained at the M06/6-31+G(d,p) level of theory.

Table S2. Energy of the optimized ground state of the five lowest-energy tautomers of BA in water, complexed with 3H$_2$O molecules, obtained at the M06/6-31+G(d,p) level of theory. Single-point energies and dipole moments are also shown in parentheses at the B3LYP/IEF-PCM/6-311++G(d,p)‖M06/6-31+G(d,p) level of theory in water for comparison with the values reported in Table S1.

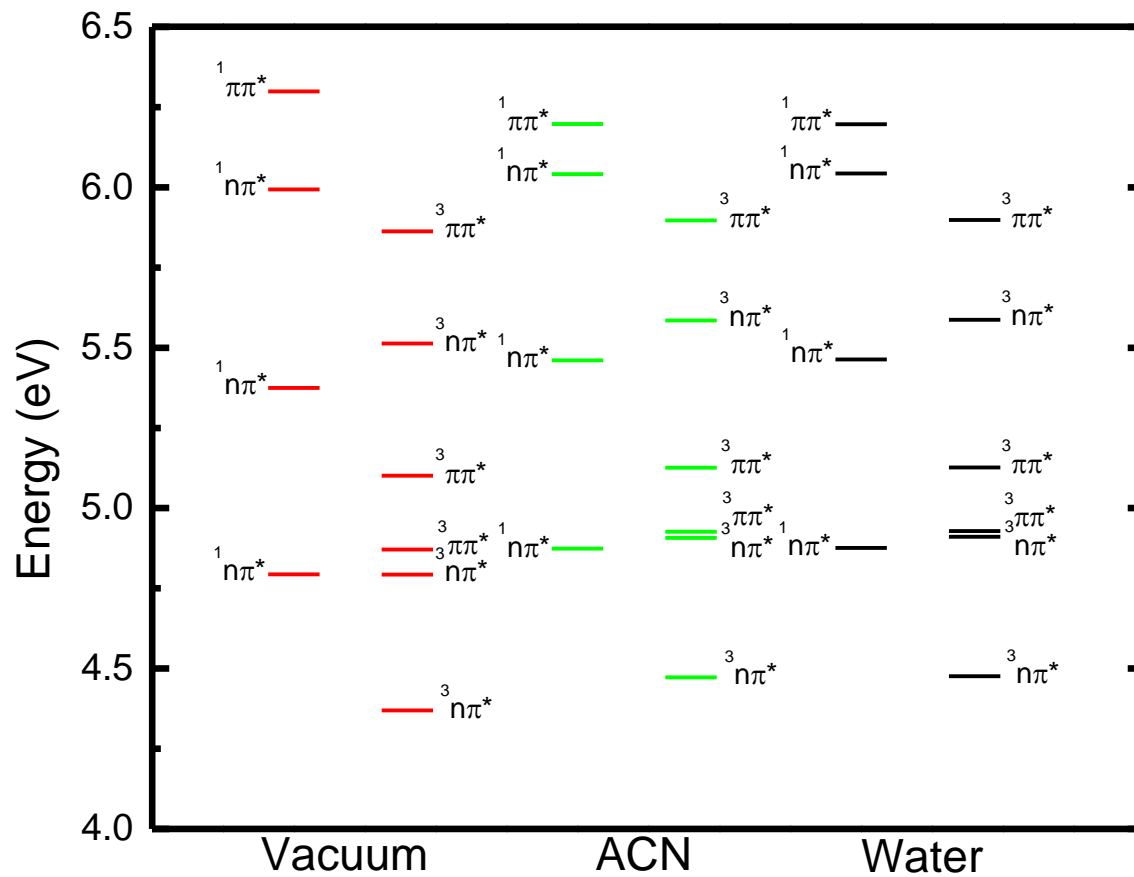| Tautomer	Energy (kJ/mol)	Dipole Moment (Debye)
1	104.6 (79.1)	5.40 (6.55)
2	54.8 (57.2)	3.21 (3.91)
3	**0.0 (0.0)**	**0.91 (1.08)**
4	47.5 (27.9)	5.98 (7.33)
5	42.5 (46.8)	1.29 (1.49)

Figure S3. Vertical excitation energies of the tri-keto tautomer of BA determined at the TD-PBE0/6-311++G(d,p) level of theory and using IEF-PCM to model the solvent where applicable.

Table S3. Vertical excitation energies of the tri-keto tautomer of BA determined at TD-PBE0/6-311++G(d,p) level of theory and IEF-PCM to model the solvent where applicable.

Character	Vacuum		ACN		Water	
	Energy (eV)	Oscillator Strength	Energy (eV)	Oscillator Strength	Energy (eV)	Oscillator Strength
$^1n\pi^*$	4.8	0.000	4.9	0.000	4.9	0.000
$^1n\pi^*$	5.4	0.000	5.5	0.001	5.5	0.001
$^1n\pi^*$	6.0	0.000	6.0	0.000	6.1	0.000
$^1\pi\pi^*$	6.3	0.130	6.2	0.168	6.2	0.168
$^3n\pi^*$	4.4		4.5		4.5	
$^3n\pi^*$	4.8		4.9		4.9	
$^3\pi\pi^*$	4.9		4.9		5.0	
$^3\pi\pi^*$	5.1		5.1		5.2	
$^3n\pi^*$	5.5		5.6		5.6	
$^3\pi\pi^*$	5.9		5.9		6.0	

3.2   *Ground-State Absorption and Tautomerization*

Figure 1a shows the ground-state absorption spectrum of BA in aqueous buffer solution at several different pHs. As the pH of the solution decreases from 7.4 to 2.0, the absorption band at 257 nm also decreases, whereas the absorption band at 210 nm increases. The molar absorptivity coefficients determined experimentally at 257 nm in neutral (19500 ± 450 $cm^{-1}M^{-1}$) and acidic (690 ± 70 $cm^{-1}M^{-1}$) conditions agree well with those reported previously.[12] The pKa value that we estimated from our data of 3.92 also agrees well with the 3.99 value determined in ref. 12 within the experimental error. The apparent isosbestic point at ~222 nm suggests that the tautomerization is occurring predominantly between two species. From our ground-state optimizations of the 16 possible tautomers of BA (Figure S1 and revised Table S1), the tri-keto tautomer is predicted to be the only species thermodynamically available at room temperature, which is clearly inconsistent with the experimental results presented in this work and in ref. 12. It is likely that this discrepancy is due to the use of an implicit water solvation model and possibly

also to the level of theory used in this work. Therefore, in an effort to account for this discrepancy, we performed preliminary micro-hydration calculations including three water molecules (Figure S2) to obtain an idea of which tautomer(s) of BA may be present in PBS at pH 7.4 at room temperature. According to Table S2 and Figure S5, one or more of the five calculated enol tautomers may explain the experimental absorption spectrum at pH 7.4, but unfortunately a concrete assignment will require the use of a larger number of water molecules and/or higher level of theory. Therefore, we conclude that an enol tautomer of BA is likely presented in solution at pH 7.4, but contrary to what is reported in the main text of our paper, we cannot unequivocally assign which enol species may be present.

In an effort to identify the major BA tautomer observed at acidic pHs, analogous experiments and calculations were performed in acetonitrile solution (Table S1 and Figure S4). The calculations suggest that the tri-keto species more energetically stable in acetonitrile than any of the other tautomers by at least 35.79 kJ/mol, which is in agreement with a previous study done in vacuum.[13] Furthermore, the good agreement of the absorption spectrum of BA at pH 2.0 and in acetonitrile with the calculated vertical energies for the tri-keto species support the hypothesis that this tautomer is the predominant species in acidic aqueous solution (Figure S4). Our analysis is in agreement with a previous investigation,[12] which suggests that an enol tautomer of BA is the predominant species at neutral pH, while it is the tri-keto form predominates at acidic pHs.
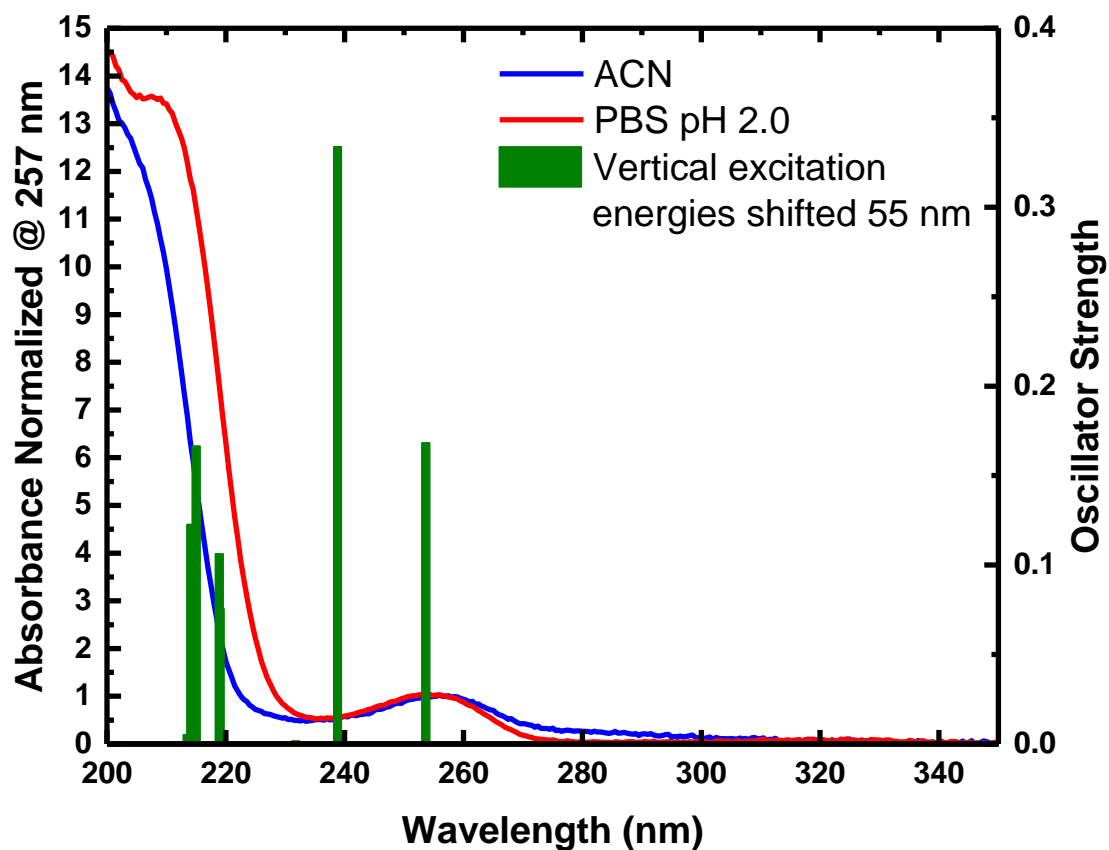
Figure S4. Ground-state absorption spectra of BA in phosphate buffer saline (PBS) solution at pH 2.0 and in acetonitrile (ACN) overlaid with the vertical excitation energies of the tri-keto tautomer of BA (shifted by 55 nm) determined at TD-PBE0/IEF-PCM/6-311++G(d,p) level of theory in water.

3.2.1 Comparison of the Ground-State Absorption Spectra of BA with the Vertical Excitation Energies of the Five Lowest-Energy Tautomers of BA Complexed with 3H₂O Molecules

Table S4. Vertical excitation energies of **Tautomer 1** of BA complexed with $3H_2O$ determined at the TD-PBE0/IEFPCM/6-311++G(d,p)||M06/6-31+G(d,p) level of theory using the water solvation model.

Character	Energy (eV)	Oscillator Strength
$^1n\pi$	5.0	0.0003
$^1n\pi$	5.3	0.001
$^1n\pi$	5.6	0.008
$^1\pi\pi$	5.8	0.092
$^1n\pi$	6.1	0.009
$^1\pi\pi$	6.2	0.094
$^1n\pi$	6.3	0.011
$^1\pi\pi$	6.5	0.270
$^1n\pi$	6.6	0.008
$^1n\pi$	7.1	0.004
$^3\pi\pi$	4.5	
$^3n\pi$	4.6	
$^3\pi\pi$	4.8	
$^3n\pi$	5.1	
$^3n\pi$	5.2	
$^3\pi\pi$	5.7	
$^3n\pi$	6.1	
$^3n\pi$	6.1	
$^3n\pi$	6.2	
$^3n\pi$	6.6	

Table S5. Vertical excitation energies of **Tautomer 2** of BA complexed with $3H_2O$ determined at the TD-PBE0/IEFPCM/6-311++G(d,p)‖M06/6-31+G(d,p) level of theory using the water solvation model.

Character	Energy (eV)	Oscillator Strength
$^1n\pi$	4.6	0.0001
$^1n\pi$	5.3	0.001
$^1\pi\pi$	5.5	0.235
$^1n\pi$	5.7	0.001
$^1n\pi$	6.2	0.013
$^1n\pi$	6.4	0.001
$^1\pi\pi$	6.7	0.001
$^1\pi\pi$	6.8	0.094
$^1n\pi$	6.8	0.001
$^1n\pi$	6.9	0.001
$^3n\pi$	4.3	
$^3\pi\pi$	4.3	
$^3n\pi$	4.9	
$^3\pi\pi$	5.2	
$^3n\pi$	5.5	
$^3\pi\pi$	6.0	
$^3n\pi$	6.2	
$^3n\pi$	6.3	
$^3\pi\pi$	6.5	
$^3\pi\pi$	6.6	

Table S6. Vertical excitation energies of **Tautomer 3 (tri-keto)** of BA complexed with $3H_2O$ determined at the TD-PBE0/IEFPCM/6-311++G(d,p)||M06/6-31+G(d,p) level of theory using the water solvation model.

Character	Energy (eV)	Oscillator Strength
$^1n\pi$	5.0	0.000
$^1n\pi$	5.6	0.001
$^1n\pi$	6.0	0.023
$^1\pi\pi$	6.1	0.148
$^1\pi\pi$	6.5	0.071
$^1n\pi$	6.6	0.008
$^1\pi\pi$	6.7	0.260
$^1n\pi$	6.9	0.003
$^1n\pi$	7.0	0.001
$^1n\pi$	7.1	0.001
$^3n\pi$	4.6	
$^3\pi\pi$	4.9	
$^3n\pi$	5.0	
$^3\pi\pi$	5.1	
$^3n\pi$	5.6	
$^3\pi\pi$	5.9	
$^3\pi\pi$	6.5	
$^3n\pi$	6.5	
$^3\pi\pi$	6.6	
$^3n\pi$	6.8	

Table S7. Vertical excitation energies of **Tautomer 4** of BA complexed with $3H_2O$ determined at the TD-PBE0/IEFPCM/6-311++G(d,p)||M06/6-31+G(d,p) level of theory using the water solvation model.

Character	Energy (eV)	Oscillator Strength
$^1\pi\pi$	5.4	0.242
$^1n\pi$	5.6	0.000
$^1n\pi$	6.0	0.003
$^1\pi\pi$	6.2	0.165
$^1n\pi$	6.5	0.0001
$^1n\pi$	6.6	0.001
$^1n\pi$	6.6	0.0004
$^1\pi\pi$	6.8	0.094
$^1n\pi$	6.9	0.001
$^1n\pi$	7.0	0.001
$^3\pi\pi$	3.9	
$^3\pi\pi$	4.9	
$^3n\pi$	5.2	
$^3\pi\pi$	5.7	
$^3n\pi$	6.0	
$^3n\pi$	6.1	
$^3\pi\pi$	6.1	
$^3n\pi$	6.5	
$^3n\pi$	6.6	
$^3\pi\pi$	6.6	

Table S8. Vertical excitation energies of **Tautomer 5** of BA complexed with $3H_2O$ determined at the TD-PBE0/IEFPCM/6-311++G(d,p)||M06/6-31+G(d,p) level of theory using the water solvation model.

Character	Energy (eV)	Oscillator Strength
$^1n\pi$	5.1	0.0001
$^1n\pi$	5.4	0.0004
$^1n\pi$	5.7	0.004
$^1\pi\pi$	5.8	0.124
$^1\pi\pi$	6.3	0.193
$^1n\pi$	6.4	0.010
$^1\pi\pi$	6.5	0.178
$^1n\pi$	6.7	0.002
$^1n\pi$	6.9	0.002
$^1n\pi$	7.1	0.003
$^3\pi\pi$	4.5	
$^3n\pi$	4.7	
$^3\pi\pi$	4.9	
$^3n\pi$	5.1	
$^3n\pi$	5.3	
$^3\pi\pi$	5.7	
$^3n\pi$	6.2	
$^3\pi\pi$	6.3	
$^3\pi\pi$	6.6	
$^3n\pi$	6.7	

Figure S5. Ground-state absorption spectra of BA in phosphate buffer saline (PBS) solution at pH 2.0 or 7.4 overlaid with the vertical excitation energies of the five lowest-energy tautomers of BA in water (Table S1), complexed with $3H_2O$ molecules, obtained at the TD-PBE0/IEF-PCM/6-311++G(d,p)||M06/6-31+G(d,p) level of theory in water. Vertical excitation energies were shifted to the red in order to better match the lowest-energy experimental absorption band of BA at pH 2 or 7.4: Tautomer 1 was shifted by 50 nm; Tautomer 2 was shifted by 30 nm, tri-keto Tautomer 3 was shifted by 50 nm, Tautomer 4 was shifted by 30 nm, and Tautomer 5 was shifted by 50 nm.

3.3   Kinetic Isotope Effect in Transient Absorption Spectroscopy of BA

Figure S6 shows normalized kinetic traces at two representative probe wavelengths for BA in non-deuterated and deuterated PBS solutions at pH 7.4. These data were collected back-to-back under otherwise identical experimental conditions. From these kinetic traces, it is apparent that the deuterated solvent has no appreciable effect on the kinetics of BA, suggesting that proton- or hydrogen-transfer pathway is not the rate-limiting relaxation pathway in the excited-state dynamics of BA.
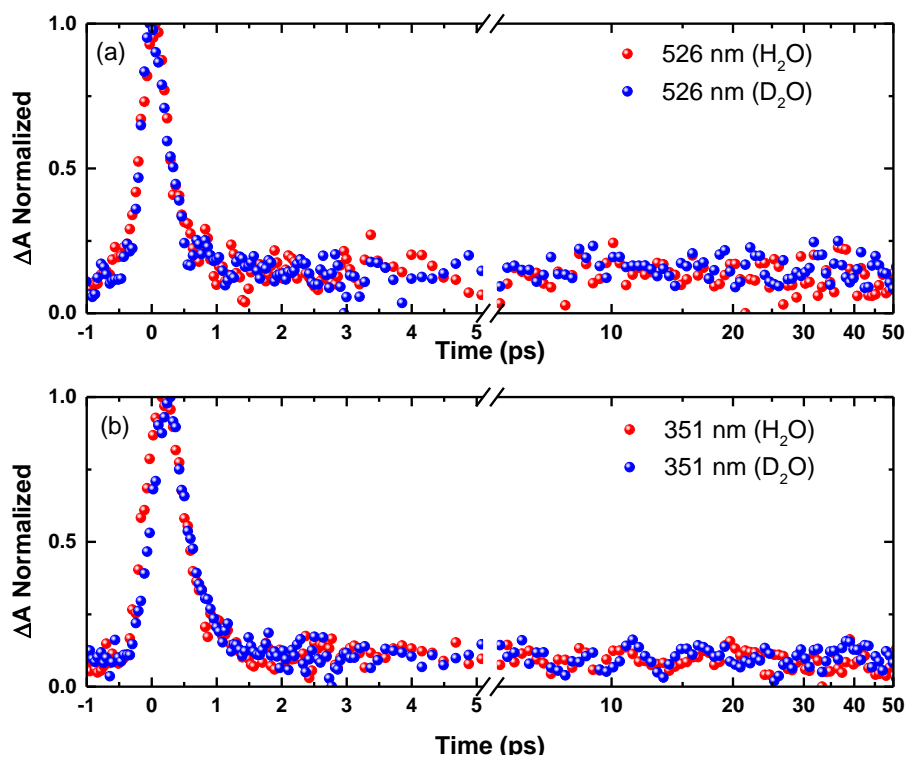
Figure S6. Normalized kinetic traces for BA in non-deuterated (H_2O) and deuterated (D_2O) buffer solutions at pH 7.4, following 268 nm excitation. No kinetic isotope effect is observed in either the visible (a) or UV (b) transient absorption bands.
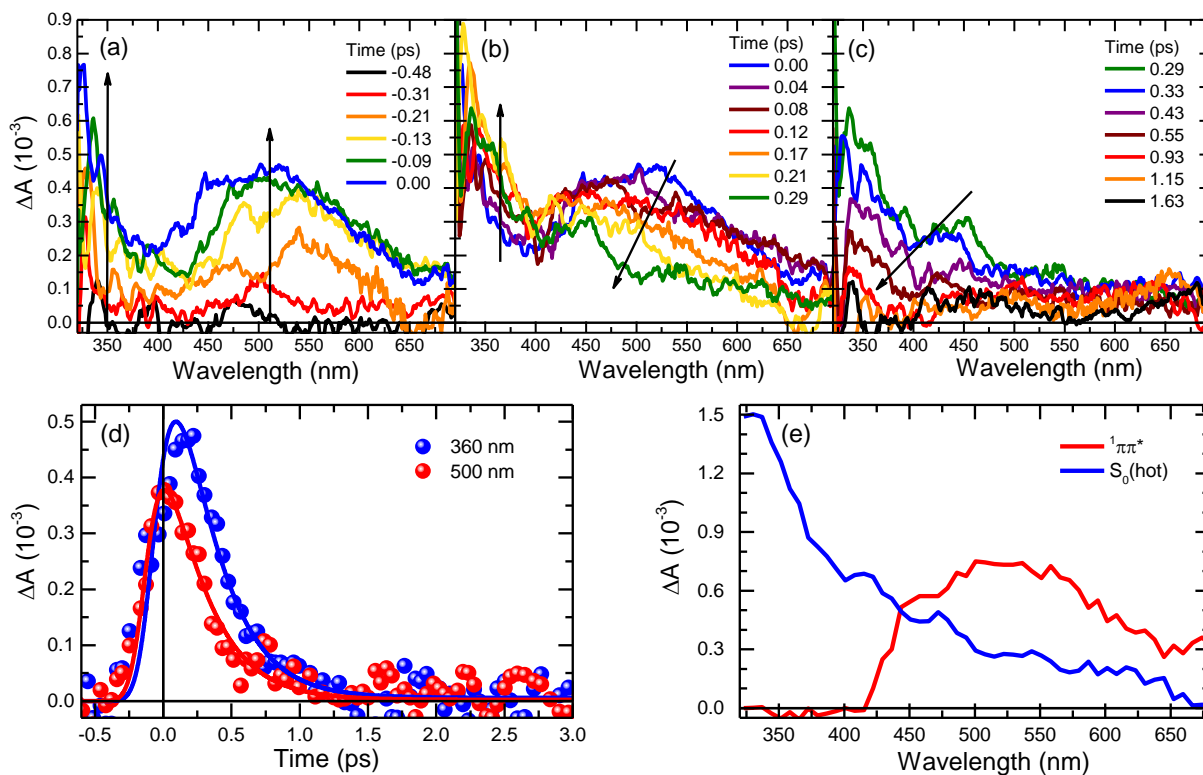
Figure S7. (a-c) Evolution of the transient absorption spectra of BA in aqueous phosphate buffer pH 2.5 over the first ~ 2 ps. **(d)** Kinetic traces taken for the UV (360 nm) and visible (500 nm) transient absorption bands and the fit lines obtained from a global analysis of the data across the full probe window using a two component sequential kinetic model. **(e)** Decay associated spectra extracted from the global analysis presenting a deconvolution and assignment of the two major transient species.

4. *2,4,6-Triaminopyrimidine*
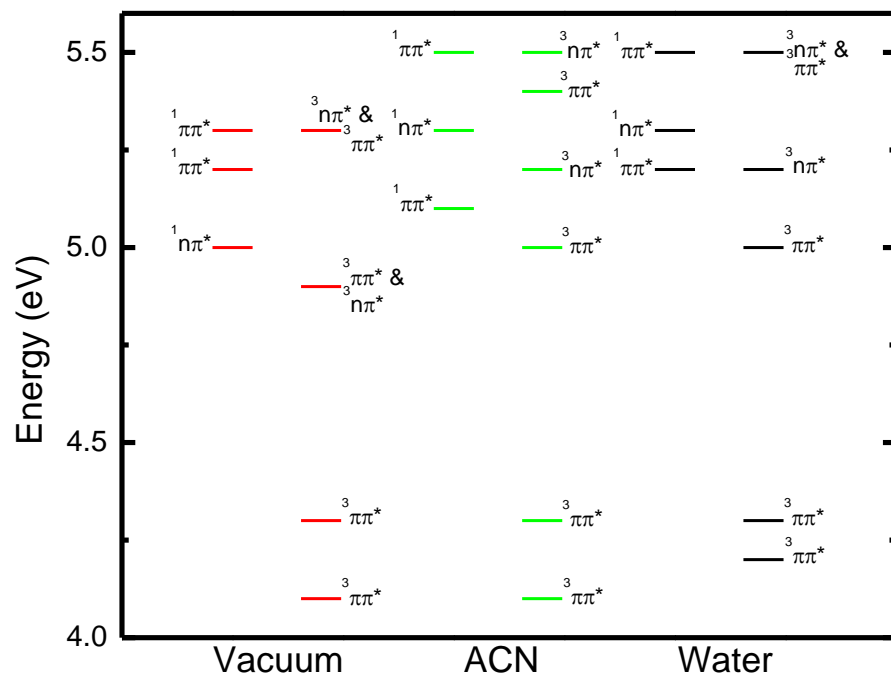
4.1 *Computational Results*

Figure S8. Vertical excitation energies of TAP determined at TD-PBE0/6-311++G(d,p) level of theory and using the IEF-PCM to model the solvent where applicable.

Table S9. Vertical excitation energies of TAP determined at TD-PBE0/6-311++G(d,p) level of theory and using IEF-PCM to model the solvent where applicable.

	Vacuum			ACN		Water	
Character	Energy (eV)	Oscillator Strength		Energy (eV)	Oscillator Strength	Energy (eV)	Oscillator Strength
$^1n\pi^*$	5.0	0.005	$^1\pi\pi^*$	5.1	0.123	5.2	0.123
$^1\pi\pi^*$	5.2	0.064	$^1n\pi^*$	5.3	0.002	5.3	0.002
$^1\pi\pi^*$	5.3	0.016	$^1\pi\pi^*$	5.5	0.121	5.5	0.120
$^3\pi\pi^*$	4.1		$^3\pi\pi^*$	4.1		4.2	
$^3\pi\pi^*$	4.3		$^3\pi\pi^*$	4.3		4.3	
$^3n\pi^*$	4.9		$^3\pi\pi^*$	5.0		5.0	
$^3\pi\pi^*$	4.9		$^3n\pi^*$	5.2		5.2	
$^3\pi\pi^*$	5.3		$^3\pi\pi^*$	5.4		5.5	
$^3n\pi^*$	5.3		$^3\pi\pi^*$	5.5		5.5	

4.2 Ground-State Absorption and State Assignments

Figure S9 depicts the ground-state absorption of TAP in both PBS at pH 7.4 and in ACN, overlaid with the computational results. The molar absorptivity obtained in PBS at pH 7.4 and in ACN were (1370 ± 140) $M^{-1}cm^{-1}$ at 270 nm and (17940 ± 440) $M^{-1}cm^{-1}$ at 265.5 nm, respectively. The vertical excitation energies suggest that the lowest energy absorption band of TAP in both water and acetonitrile is composed of two $^1\pi\pi^*$ states and one $^1n\pi^*$ state; the latter

exhibiting a very small oscillator strength around 272 nm in Figure S8. Although the calculations predict that the ^{1}nπ* state is slightly higher in energy than the lowest-energy ^{1}ππ* state, it is possible that the ^{1}nπ* state could be isoenergetic or even lower in energy that the lowest-energy ^{1}ππ* state at higher levels of theory, as observed for other nucleobases.
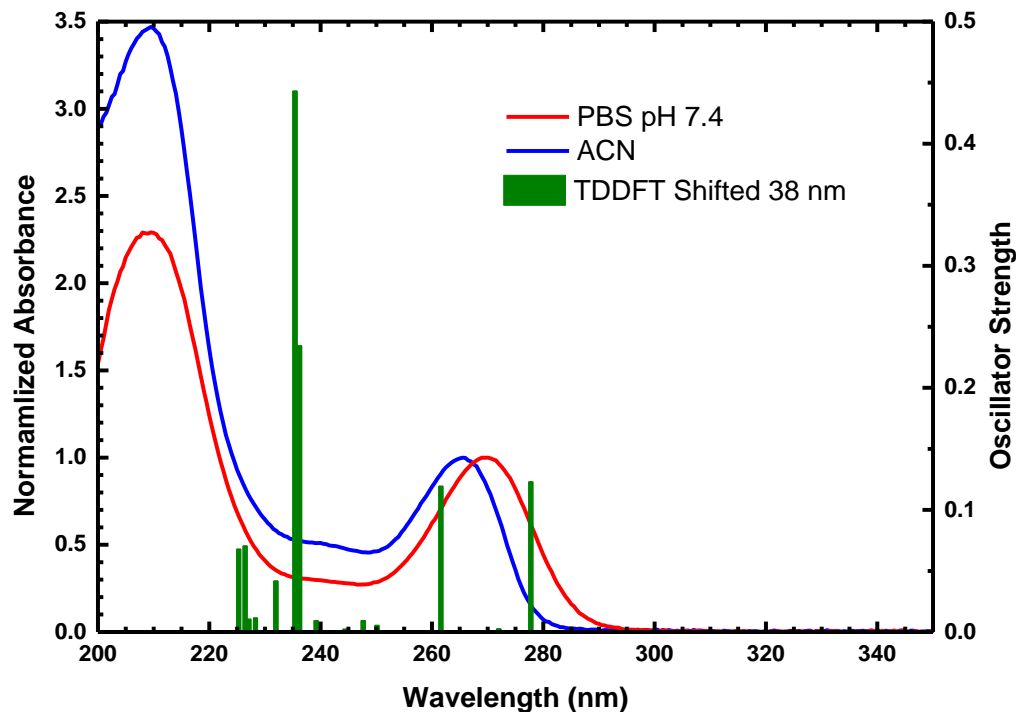

Figure S9. Ground-state absorption spectra of TAP in phosphate buffer saline (PBS) solution at pH 7.4 and in acetonitrile (ACN), normalized at their lowest energy absorption peak and overlaid with the vertical excitation energies of TAP (shifted by 38 nm) determined at the TD-PBE0/IEF-PCM/6-311++g(d,p) level of theory in water.

5.   *References*

1   C. Reichardt, R. A. Vogt and C. E. Crespo-Hernández, *J. Chem. Phys.*, 2009, **131**, 224518.

2   M. Pollum, S. Jockusch and C. E. Crespo-Hernández, *J. Am. Chem. Soc.*, 2014, **136**, 17930–17933.

3   M. M. Brister and C. E. Crespo-Hernández, *J. Phys. Chem. Lett.*, 2015, **6**, 4404–4409.

4   M. Rasmusson, A. N. Tarnovsky and E. Akesson, *Chem. Phys. Lett.*, 2001, **335**, 201–208.

5   C. E. Crespo-Hernández and B. Kohler, *J. Phys. Chem. B*, 2004, **108**, 11182–11188.

6   M. J. Frisch, G. W. Trucks, H. B. Schlegel, G. E. Scuseria, M. A. Robb, J. R. Cheeseman, G. Scalmani, V. Barone, B. Mennucci, G. A. Petersson, H. Nakatsuji, M. Caricato, X. Li, H. P. Hratchian, A. F. Izmaylov, J. Bloino, G. Zheng, J. L. Sonnenberg, M. Hada, M. Ehara, K. Toyota, R. Fukuda, J. Hasegawa, M. Ishida, T. Nakajima, Y. Honda, O. Kitao, H. Nakai, T. Vreven, J. Montgomery, J. A., J. E. Peralta, F. Ogliaro, M. Bearpark, J. J. Heyd, E. Brothers, K. N. Kudin, V. N. Staroverov, R. Kobayashi, J. Normand, K. Raghavachari, A. Rendell, J. C. Burant, S. S. Iyengar, J. Tomasi, M. Cossi, N. Rega, N. J. Millam, M. Klene, J. E. Knox, J. B. Cross, V. Bakken, C. Adamo, J. Jaramillo, R. Gomperts, R. E. Stratmann, O. Yazyev, A. J. Austin, R. Cammi, C. Pomelli, J. W. Ochterski, R. L. Martin, K. Morokuma, V. G. Zakrzewski, G. A. Voth, P. Salvador, J. J. Dannenberg, S. Dapprich, A. D. Daniels, Ö. Farkas, J. B. Foresman, J. V. Ortiz, J. Cioslowski and D. J. Fox, 2009.

7   V. Barone, M. Cossi and J. Tomasi, *J. Chem. Phys.*, 1997, **107**, 3210-3221.

8   E. Cancès, B. Mennucci and J. Tomasi, *J. Chem. Phys.*, 1997, **107**, 3032-3041.

9   Y. Zhao and D. G. Truhlar, *Theor. Chem. Acc.*, 2008, **120**, 215-241.

10   C. Adamo, G. E. Scuseria and V. Barone, *J. Chem. Phys.*, 1999, **111**, 2889–2899.

11   C. Adamo and V. Barone, *J. Chem. Phys.*, 1999, **110**, 6158–6170.

12   A. G. Briggs, J. E. Sawbridge, P. Tickle and J. M. Wilson, *J. Chem. Soc. B Phys. Org.*, 1969, **6**, 802–805.

13   Y. Valadbeigi, H. Farrokhpour and M. Tabrizchi, *Chem. Phys. Lett.*, 2014, **601**, 155–162.